

Crystallization by settling in suspensions of hard spheres

Bruce J. Ackerson,* S. E. Paulin, and Benjamin Johnson

Department of Physics, Oklahoma State University, Stillwater, Oklahoma 74078

William van Meegen and Sylvia Underwood

Department of Applied Physics, Royal Melbourne Institute of Technology, Melbourne, Victoria 3000, Australia

(Received 29 June 1998)

We examine crystallization by settling for two different model hard-sphere suspensions. Sedimentation velocities, internal shock velocities, and crystal growth velocities are measured. Dynamic light scattering experiments measure volume fraction profiles in fluid phases, while Bragg scattering experiments determine volume fraction profiles in crystal phases. Centrifugation experiments determine the particle Péclet number above which samples will not crystallize. The sedimentation velocities, as a function of volume fraction, agree with other “hard-sphere” data. Remarkably, the value of the reduced crystal growth velocity (~ 0.075) obtains for two orders of magnitude of the particle Péclet number. Kynch theory provides an adequate description of the data in the fluid phase, but is less adequate for volume fraction profiles in the crystal phase. The crystals in the dense sediment are compressed more along a vertical axis relative to the horizontal axis. Predicted Wilson-Frenkel crystal growth velocities, calculated using known hard-sphere equations of state and a short-time self-diffusion constant, rationalize the measured crystal growth velocities. [S1063-651X(99)05806-7]

PACS number(s): 64.70.Dv, 81.10.Fq, 82.70.Dd

I. INTRODUCTION

The growth of colloidal crystals has been studied in a variety of systems [1–6]. The crystal radius grows linearly with time [2–4] following homogeneous or heterogeneous nucleation in suspensions of charge-stabilized particles. The Wilson-Frenkel growth law provides an explanation for these data. In suspensions of hard spheres, the crystal radius grows with a quasi-power-law behavior in time with an exponent typically between $\frac{1}{2}$ and unity [6,7] following homogeneous nucleation. For hard spheres the volume fraction differs by 10% between the crystal and liquid in the coexistence region. Thus crystal growth in the coexistence region depletes the surrounding metastable liquid in the immediate neighborhood of the crystal. A depletion zone also develops for metastable fluid volume fractions above the melting value if the osmotic pressure balance across the liquid crystal interface produces a relatively larger crystal volume fraction compared to the fluid. The depletion zone leads to diffusion-limited growth [8] with growth exponent $\frac{1}{2}$ when particle incorporation rates into the crystal are large. Otherwise the crystal growth is not fully interfaced or diffusion limited but has a transient quasi-power-law growth. The depletion process masks observation of the Wilson-Frenkel growth law for hard-sphere crystals and can be determined only indirectly [8].

Alternatively, at volume fractions less than the freezing value, crystals have been observed to grow as long columns in the accumulating sediment of colloidal suspensions. The crystal growth rates are linear in time even for “hard-sphere” suspensions because the gravitational settling of the metastable fluid to the crystal boundary provides a steady

source of material. Evidently, no diffusion-limited depletion zone develops. Davis and Russel have studied this sedimentation process both theoretically and experimentally [9–12]. They assume a linear growth velocity given by the Wilson-Frenkel law and governed by the volume fraction of the metastable fluid in contact with the growing crystal interface. For hard spheres the growth velocity of the crystal increases with increasing volume fraction of the metastable fluid above the freezing value due to the increase of thermodynamic driving forces with increasing quench depth. However, viscous loss terms, due to hydrodynamic interactions, reduce the crystal growth velocity as the volume fraction increases above (approximately) the crystal melting value and towards the glass. If the flux of settling particles is greater than that which the maximum crystal growth velocity can accommodate, a glassy sediment results. Otherwise, there is a range of stable growth velocities from zero at the freezing point to the maximum velocity near the melting point. In principle, by controlling the rate of settling by centrifugation, one can test the Wilson-Frenkel growth theory.

We present data for two different suspensions of hard spheres that have larger particle Péclet numbers (Pe_p) than previously reported though the sample Péclet value (Pe) is within the same range of earlier studies [9]. Measured sedimentation velocities indicate that these samples better approximate hard-sphere suspensions than earlier studies [9]. Kynch theory rationalizes observations in the fluid phase. We extend the Kynch theory into the crystal phase. The compressibility gradient is sufficiently large that this solution is not as good an approximation as that for the overlying fluid phase. However, the Kynch result is the zeroth-order solution for large Péclet number expansions. The Wilson-Frenkel growth law, with improved approximations for the fluid and solid equations of state and for the self-diffusion kinetic coefficient, provides an explanation for our observations of crystal growth. This theory predicts a very narrow range of

*Author to whom correspondence should be addressed. Electronic address: bjack@osuunx.ucc.okstate.edu

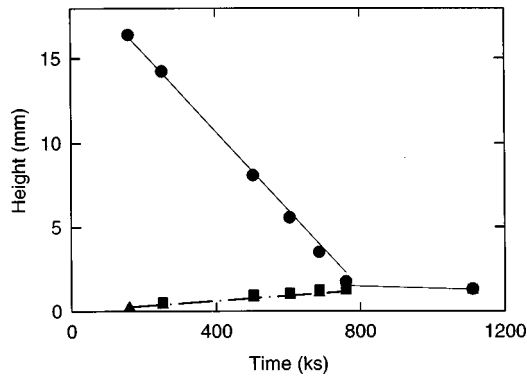


FIG. 1. Feature height versus time for a 380-nm particle sample with initial volume fraction 0.041. The filled circles represent the boundary between the disordered particle suspension and the clear supernatant. The triangles represent the boundary between the disordered particle suspension and the ordered crystal phase. Kynch theory predicts lines shown for times less than 800 ks.

values for the experimentally measured reduced crystal growth velocities, consistent with observation.

II. EXPERIMENTAL METHODS AND RESULTS

We report data for two different model hard-sphere systems. A thin layer (~ 10 nm) of poly-12-hydroxystearic acid stabilizes the larger 500-nm radius polymethyl-methacrylate core particles from aggregation. A mixture of decalin and tetralin suspends the particles and is tuned to match the particle refractive index, rendering the samples transparent. Static light scattering measurements show the polydispersity to be less than 5% relative standard deviation. The particle Péclet value is $Pe_p = U_0 R / D_0 = 0.165$. Here R is the particle radius and $U_0 = 2 \Delta \rho R^2 g / 9 \eta$ is the dilute limit sedimentation velocity. $\Delta \rho$ is the difference between particle and solvent density, g is the acceleration of gravity, and η is the solvent viscosity. $D_0 = k_B T / 6 \pi \eta R$ is the dilute solution particle diffusion constant, where $k_B T$ is the thermal energy. The smaller 380-nm-radius particles have cores of copolymer of methylmethacrylate and tri-fluoroethylacrylate with a stabilizing coating of poly-12-hydroxystearic acid as well. The suspending solvent, cis-decalin, matches the particle index of

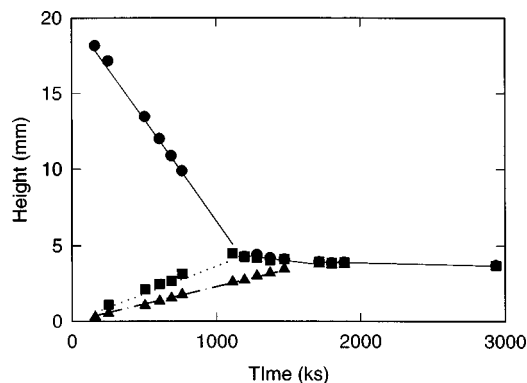


FIG. 2. Feature height versus time for a 380-nm particle sample with initial volume fraction 0.124. The symbols are the same as in Fig. 1. The solid squares represent the position of a fluid shock. Kynch theory predicts the lines for times less than approximately 1000 ks.

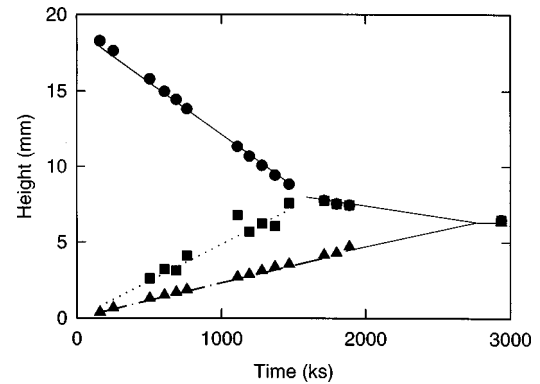


FIG. 3. Feature height versus time for a 380-nm particle sample with initial volume fraction 0.22. The symbols have the same meaning as in Figs. 1 and 2. Kynch theory predicts the lines shown for times less than approximately 1500 ks.

refraction. The polydispersity is 5%, as determined by dynamic light scattering, and $Pe_p = 0.048$. The particle Péclet numbers range nearly an order of magnitude larger than those for the systems investigated by Davis and Russel [9]. Yet these systems still evidence columnar crystal growth. Previous investigations of our systems reveal hard-sphere behavior [5–7,13]. This earlier work includes determining the hard-sphere phase transition and referencing reported volume fractions to the accepted theoretical freezing value [13,14]. These experiments determine the core volume fractions of the freezing and melting points for each system. Scaling the volume fractions so the freezing core volume fraction corresponds to that determined via computer simulation, $\phi_{\text{freeze}} = 0.494$, determines the volume fraction reported [14]. The ratio of the reported volume fractions to those determined directly by weighing is 1.15 for the 380-nm-radius particles and 1.04 for the 500-nm-radius particles.

Rectangular cuvettes ($1 \times 1 \times 5$ cm³) hold individual samples of each particle size and span a range of volume fractions. Mechanical tumbling, end for end as much as 24 h, mixes the samples thoroughly. Particles settle in stationary cuvettes stood upright and subjected to ambient room temperature. The temperature for any given run varied by no more than one-half degree. For comparison of different runs, we report data corrected to 20 °C. In time the samples develop shock fronts, regions where the particle volume frac-

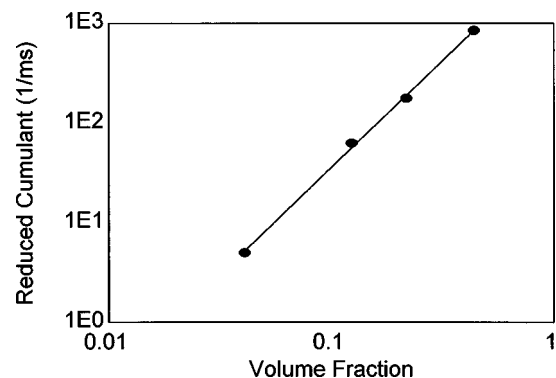


FIG. 4. Dynamic light scattering first cumulant minus the theoretical dilute limit cumulant versus volume fraction for homogeneous samples of 380-nm particles.

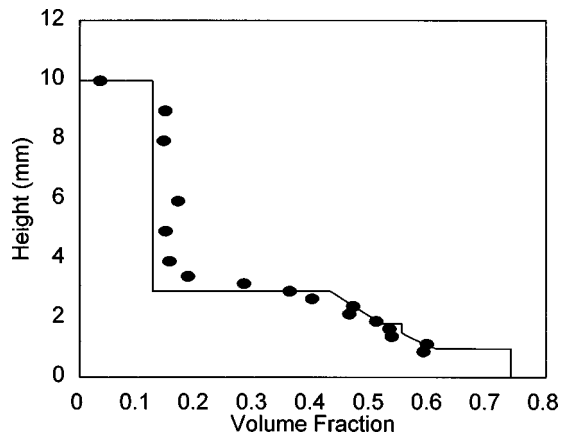


FIG. 5. Height versus volume fraction for a 380-nm particle sample with initial volume fraction 0.124 after settling for 680 ks. The solid lines are the prediction of Kynch theory.

tion changes rapidly with vertical height. We measured the position of these shock fronts as a function of elapsed time, using a telescope mounted on a vernier capable of reading to $10\text{-}\mu\text{m}$ accuracy. Figures 1–3 show height versus elapsed time data for the smaller radius particle samples at volume fractions $\phi=0.041, 0.124,$ and $0.22,$ respectively. The uppermost line in each figure marks the boundary between the pure solvent above from the uniform distribution of particles setting below. The particle volume fraction in this lower region equals the initial value. The slope of this boundary line determines the sedimentation velocity U . The lowest boundary line separates the growing crystal from the fluid phase above. The slope of this line determines the crystal growth velocity U_c . For samples with initial volume fractions above ~ 0.1 , there is another shock boundary, where the fluid phase volume fraction changes abruptly. Above this boundary, the initial sample volume fraction obtains, while below this boundary the sample volume fraction increases with decreasing height in the sample. This region is the “fan” because lines of constant volume fraction in Kynch theory extrapolate through the origin (or fan out from the origin) in this region. For volume fractions below ~ 0.1 , no fan is observed. We also monitored the air-sample meniscus height. This height decreased with time, indicating solvent evaporation.

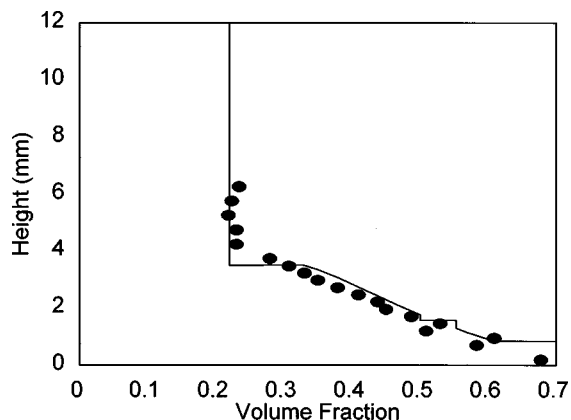


FIG. 6. Height versus volume fraction for a 380-nm particle sample with initial volume fraction 0.22 after settling for 760 ks. The solid lines are predicted by Kynch theory.

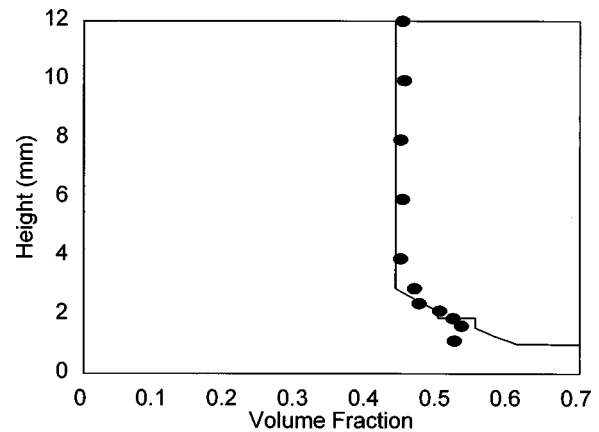


FIG. 7. Height versus volume fraction for a 380-nm particle sample with initial volume fraction 0.44 after settling for 765 ks. The solid lines are predicted by Kynch theory.

The evaporation does not influence the dynamics of settling, but does increase the initial volume fraction of the sample if it is mixed again for any subsequent runs.

We measured the first cumulant of the dynamic light scattering (DLS) correlation function [15] using a helium neon laser at 90° scattering angle for selected smaller particle samples having uniform density. Thorough tumbling of these samples prior to measurement homogenized any density variations. The measurements determine the monotonic function shown in Fig. 4, which correlates sample volume fraction with the measured first cumulant minus the theoretical cumulant value at zero-particle concentration. In this way cumulant measurements as a function of height for heterogeneous samples give the volume fraction as a function of height. The height resolution is $300\ \mu\text{m}$, the width of the focused incident laser beam in the sample. Figures 5–7 show this density as a function of height for the three volume fractions $\phi=0.124, 0.22,$ and 0.44 after settling for 680, 760, and 765 ks respectively. We do not expect this mapping to work for the crystal phase (volume fractions greater than

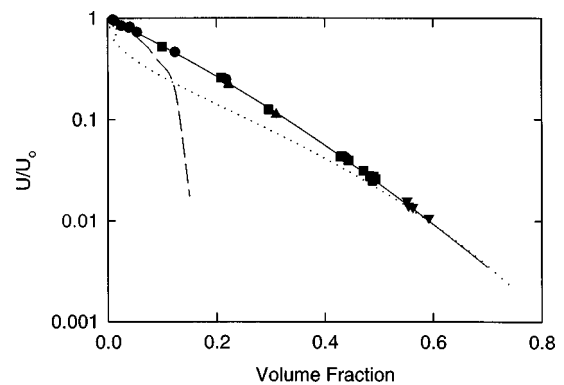


FIG. 8. Reduced sedimentation velocity as a function of volume fraction for the 380-nm particle samples (circles and triangles) and the 500-nm particle samples (squares) for initial volume fractions less than the freezing value and (inverted triangles) for initial volume fractions greater than the melting value. The solid line is the fitted form given by Eq. (3) and the dotted line is the Zick-Homsey result for a settling fcc crystal. The long-dashed line gives the Batchelor result.

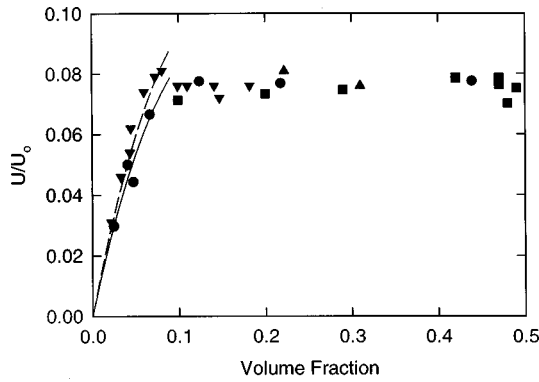


FIG. 9. Reduced crystal growth velocity shown as a function of the initial sample particle volume fraction. The inverted triangles are Davis-Russell data with $Pe_p = 0.001-0.023$. The squares are data for the 500-nm particles in this study with $Pe_p = 0.165$. The triangles and circles are data for the 380-nm particles in this study with $Pe_p = 0.048$. The dashed and solid lines are the predicted growth velocities given by Eq. (9) for sediments with $\phi_{\max} = 0.65$ and 0.74 , respectively. For $\phi > 0.1$ reduced velocities lie between 0.07 and 0.08 .

0.55) because the volume fraction correlation is done with respect to fluid phases only.

Figure 8 shows the sedimentation velocity as a function of volume fraction for both particle types with data normalized by the dilute limiting sedimentation velocity U_0 for each particle type. These data are determined from the slope of the uppermost shock in each sample as described above. Figure 9 shows the crystal growth velocity determined from the slope of the liquid-crystal boundary line. Below the freezing volume fraction ϕ_{freeze} the crystals in the dense sediment grow as columns, extending as long pillars from the cell bottom to the liquid-crystal interface. The columns are not identical in thickness, but we determine an average column width by counting the number of columns that span a certain distance (~ 2 mm) in the sample and dividing that distance by the number of columns counted. Figure 10 shows the average column width as a function of initial volume fraction for two slightly different measurement techniques.

Light diffraction from the crystal sediment of the 500-nm particle systems evidences a distorted crystal lattice. The first-order Bragg scattering angle varies both as a function of height in the sample and as a function of the scattering plane

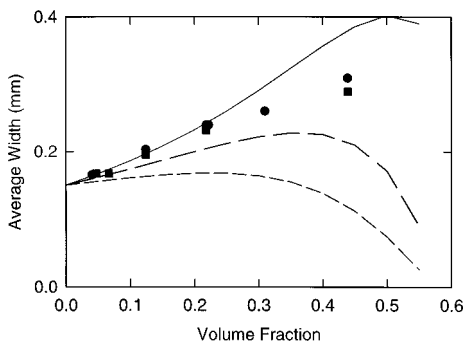


FIG. 10. Average crystal width for 380-nm particle samples as a function of volume fraction. The solid curve represents width estimates using the long-time self-diffusion coefficient and the dashed curves two different short-time self-diffusion coefficients.

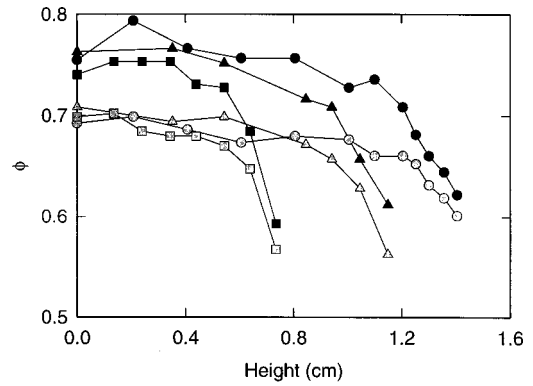


FIG. 11. Bragg scattering estimates of crystal volume fraction as a function of height in the sample of 500-nm particles. The squares, triangles, and circles correspond to 15, 27, and 35 days after mixing, respectively. A vertical axis is coplanar with the scattering plane for the solid symbols and perpendicular to the scattering plane for the grey (lower) symbols. The initial volume fraction is 0.42 . The connecting lines are a guide to the eye.

with respect to the vertical direction. At particle volume fractions greater than 0.50 , the hard-sphere freezing value, crystals nucleate and grow homogeneously in the bulk before settling and being incorporated into a dense crystal sediment. The crystal structure is a registered random stacking of close-packed layers of particles [25]. The layers correspond to (111) planes in a fcc crystal if all the stacking faults are eliminated in favor of a pure fcc form. The lowest-order powder pattern diffraction maximum results from reflections from these planes and the scattering angle is related to the separation of these planes. In Figs. 11 and 12 the volume fraction is plotted based on the measured layer separation a , where $\phi = 2.31V_{\text{sphere}}/a^3$ and V_{sphere} is the volume of a sample particle. Of course, this volume fraction assumes the crystals are not distorted, while the measured a values change with orientation and indicate the crystals are distorted. Corrections must be made for refraction of the light at the sample boundaries.

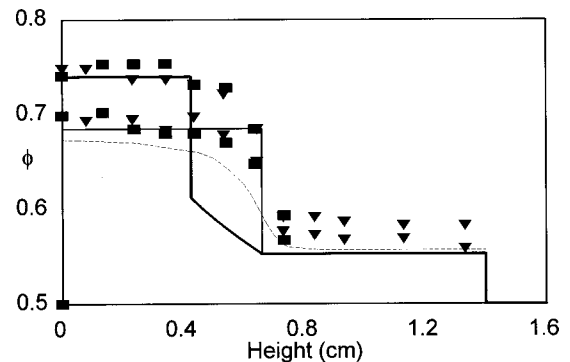


FIG. 12. Bragg scattering estimates of crystal volume fraction at 15 days after mixing as a function of height in samples of 500-nm particles. The initial volume fractions are 0.42 in the fluid phase (squares as in Fig. 11) and 0.50 in the coexistence region (triangles). A vertical axis is coplanar with the scattering plane for the solid symbols and perpendicular to the scattering plane for the grey (lower) symbols. The thick and thin solid curves are Kynch theory predictions for maximum volume fractions 0.74 and 0.685 , respectively. The dashed line is a solution to Eq. (13) having velocity 0.0695 and maximum crystal volume fraction 0.68 .

Figure 11 presents results for a sample with an initial volume fraction $\phi=0.42$. Here columnar crystals form and grow up from the bottom. The Bragg scattering indicates that the crystal is near maximum packing except near the top where the volume fraction decreases. The measured lattice constant is smaller for those (111) planes not perpendicular to the vertical axis. The crystal profile is shown for 15, 27, and 35 days after mixing. Figure 12 presents results for a sample in the coexistence region with an initial volume fraction $\phi=0.50$ and for the $\phi=0.42$ sample shown in Fig. 11 at 15 days. For the larger volume fraction sample the crystals nucleate homogeneously in the bulk and settle. At 15 days there is a dense compressed and anisotropic sediment growing up from the bottom with a fairly uniform but less dense crystal having volume fraction near the coexistent value $\phi_{\text{melt}}=0.545$ settling down from above. Note the similarity of the density profile where the two volume fractions overlap.

Settling experiments for greater than one earth gravity ($1g$) were performed using a modified swinging rotor table top centrifuge. A swinging rotor ensures that the particle acceleration direction is parallel to the vertical axis of the sample cells. This avoids the boycott effect and global convection present with a fixed rotor. The swinging arm was lengthened so that the variation in the particle acceleration over the length of the sample is less than 10% of the maximum acceleration (gravitational plus centrifugal). Samples were mixed by tumbling thoroughly overnight and then either centrifuged immediately or left to settle until a small amount of crystal begins to accumulate at the cell bottom before centrifugation. This was done to ensure that we were testing the rate of crystal growth rather than simply the rate of nucleation.

III. DISCUSSION

Davis and Russel [10] proposed a theory for the sedimentation of hard spheres based on a one-dimensional continuity equation for the conservation of sphere number. They assume the particle volume fraction ϕ to vary with height in the sample but otherwise to be uniform. The continuity equation is

$$\frac{\partial \phi}{\partial t'} + \frac{\partial U_0 f}{\partial x'} = 0, \quad (1)$$

where $U_0 f$ is the particle flux. Both convective and diffusive terms contribute to the flux as

$$U_0 f(\phi) = -\phi U_0 K(\phi) - D_0 K(\phi) \frac{d}{d\phi} [\phi Z(\phi)] \frac{d\phi}{dx'}. \quad (2)$$

In the convective term, the first term on the right-hand side of Eq. (2) U_0 is the dilute limit sedimentation velocity defined previously and $U = U_0 K(\phi)$ is the sedimentation velocity at finite volume fraction. Figure 8 shows a nearly exponential dependence of the reduced sedimentation velocity on volume fraction. The functional form

$$K(\phi) = \exp[-\phi(6.0 + 3.0\phi)], \quad (3)$$

shown as a solid line Fig. 8, gives a good fit to the data. While this functional form fits the data as a whole, the functional form $K(\phi) = \exp[-\phi(5.5 + 4.0\phi)]$ gives a better fit to the smaller particle data. The small volume fraction expansion for either of these forms deviates from the ‘‘exact’’ results calculated by Batchelor [16] for hard spheres, $K(\phi) = 1 + 6.55\phi + O(\phi^2)$, shown as the long-dashed curve in Fig. 8. The experimental deviation from the Batchelor result is not deemed significant given the simplicity of the fitting form.

Also shown in this figure, as a dotted curve, is the predicted sedimentation velocity for a face-centered-cubic crystal lattice [17]. The particles are assumed fixed rigidly in position in this theoretical calculation. In the region where the crystal is thermodynamically stable, the sedimentation velocities for the metastable fluid [Eq. (3)], the Zick-Homsey prediction for a rigid fcc lattice, and the measured crystal sedimentation velocities are remarkably similar. Experimentally, the particles are not rigidly fixed in position. In this volume fraction range the crystals nucleate homogeneously in the bulk and form a mass of finite-size randomly oriented, settling crystals.

The diffusion term in Eq. (2) accounts for particle diffusion, the effect of interparticle direct interactions, and hydrodynamic interactions. This term includes the dilute limit diffusion constant D_0 and the compressibility factor $Z(\phi) = \Pi/nk_B T$, where Π is the osmotic pressure and $n = 3\phi/4\pi R^3$ is the particle number density. The compressibility factor is evaluated using the equation of state for hard spheres. For the fluid phase we use a fit to the Carnahan-Starling equation [18]

$$Z_f(\phi) = \frac{0.904}{(\phi - 0.731)^2 + 0.0160} \quad (4)$$

and for the crystal phase the Hall form [19] for a face-centered-cubic crystal

$$Z_c(\phi) = \frac{2.17}{0.738 - \phi}. \quad (5)$$

Further details related to the chemical potential of the fluid and crystal phases and the volume fraction of fluid and crystal phases in osmotic equilibrium are given elsewhere [8]. The approximation in Eq. (4) gives a good fit to the Carnahan-Starling equation and does not diverge at random close packing $\phi=0.638$.

If we scale distance and time to the height of the sample H_0 , dimensionless variables are introduced as

$$x = x'/H_0, \quad t = U_0 t'/H_0 \quad (6)$$

and the continuity equation becomes

$$\frac{\partial \phi}{\partial t} - \frac{\partial}{\partial x} [\phi K(\phi)] = \frac{1}{\text{Pe}} \frac{\partial}{\partial x} \left(K(\phi) \frac{d}{d\phi} [\phi Z(\phi)] \frac{\partial \phi}{\partial x} \right). \quad (7)$$

This equation holds for $0 < x < 1$ with the *sample* Péclet number given by $\text{Pe} = U_0 H_0 / D_0$. The flux is zero, $f(\phi)$

=0, at the top ($x=1$) and bottom ($x=0$) of the sample. Approximate solutions of Eq. (7) describe much of the observed data [9].

A. Kynch theory

The sample Péclet number Pe is much greater than unity (~ 2500 for the smaller particles and ~ 6600 for the larger particles) such that the term on the right-hand side of Eq. (7) may be set to zero provided the compressibility factor and the change of volume fraction with height in the shock boundaries are not too large. When the diffusion term on the right-hand side of the equation is neglected, Kynch theory [9] results. This theory requires two experimental inputs, the reduced sedimentation velocity given in Fig. 8 and the volume fraction of the crystal or dense sediment ϕ_{\max} accumulating at the sample bottom. The dense sediment is assumed uniform in volume fraction.

The maximum possible ϕ_{\max} for hard spheres is 0.74, which obtains for fcc, hexagonal-close-packed, or random stacked [20] crystalline structures. However, experimental estimates of ϕ_{\max} give smaller values. This results, in part, from inefficient packing of particles in the interfacial regions between crystals having different orientations in the columnar or polycrystalline structures. Furthermore, the anisotropy observed by Bragg scattering suggests that crystals are distorted in the dense sediment. The particles are more widely separated (not close packed) in the horizontal direction as compared to the vertical direction. Finally, the hydrodynamic drag forces increase as particle surfaces come close to contact. Thus the time scale for closest packing may be large.

There are a number of ways to estimate the maximum crystal volume fraction. For the sample shown in Fig. 1, the downward flux of particles ϕU must equal the accumulation of dense sediment that is assumed of uniform volume fraction $(\phi_{\max} - \phi)U_c$. While computer simulations indicate that particle polydispersity increases the value of the volume fraction at freezing [21], we have assumed the arrival of identically sized particles with $\phi = 0.041$ for this sample. The sedimentation velocity U is determined from the slope of a straight line fitted to the data represented by the circles in Figs. 1–3. The crystal growth velocity U_c is determined from the slope of a straight line fitted to the data represented by the triangles. These assumptions and measurements give $\phi_{\max} = 0.041(1 + U/U_0) = 0.67 \pm 0.02$. Alternatively, ϕ_{\max} is estimated from $\phi_{\max} = 0.041(H_0/H_F) = 0.68 \pm 0.01$, where H_0 is the initial height of the sample, determined from the sedimentation velocity fit and extrapolation to zero elapsed time, and H_F is the final crystal height measured at long times. Because the samples shown in Figs. 2 and 3 evidence fans, the former method of estimating the maximum crystal volume fraction is not valid. The latter estimate gives $\phi_{\max} = 0.70 \pm 0.01$ and 0.670 ± 0.01 , respectively, assuming the last data point for each series represents a fully compressed and uniform crystal. Further compression will produce larger estimates and this may be especially true for the $\phi = 0.22$ sample. The estimated maximum volume fraction values are less than 0.74.

Kynch theory utilizes the flux curve given by $\phi K(\phi)$ as shown in Fig. 13. The data are obtained from Fig. 8 by multiplying reduced sedimentation velocities by correspond-

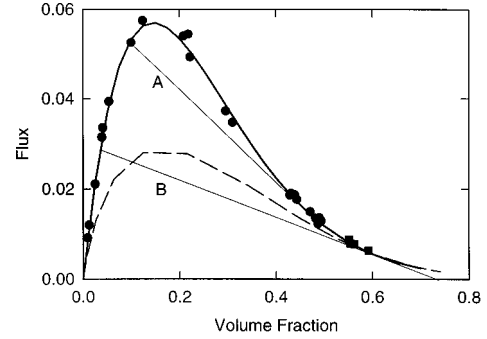


FIG. 13. Particle flux data (filled circles) for both the 380-nm particle and 500-nm particle samples as a function of volume fraction. The squares are flux data for polycrystalline sediments of 500-nm particles in the coexistence region. The solid curve is derived from Eq. (3). The dashed curve is the flux for a fcc crystal determined by Zick and Homsey. The straight line A represents a shock separating the initial volume fraction from a denser volume fraction at the top of a fan. The straight line B represents a shock separating the initial volume fraction from a dense sediment at $\phi_{\max} = 0.74$.

ing volume fractions to obtain the particle flux. Similarly, the solid curve obtains from the fitted form given in Fig. 8. The dashed curve is the flux for a fcc crystal predicted by Zick and Homsey [17]. The squares are experimentally determined flux values for a polycrystalline sediment in the coexistence region [14].

The lines shown in Figs. 1–3 represent positions in the sample where the volume fraction undergoes a rapid change with height. In Kynch theory, which neglects particle diffusion, this change is discontinuous. Except for fan regions, the volume fraction is uniform on either side of the discontinuities or “shocks.” Conservation of particle number predicts the dimensionless shock speed as

$$U_{\text{shock}} = - \frac{[\phi_1 K(\phi_1) - \phi_2 K(\phi_2)]}{[\phi_1 - \phi_2]}, \quad (8)$$

where ϕ_1 and ϕ_2 are sample volume fractions on either side of the shock boundary. Simply put, the speed of the shock times the volume fraction difference across the shock equals the net flux of particles into the shock region to maintain particle conservation locally.

Shocks are represented as straight lines on the flux curve graph. For example, the tie line B in Fig. 13 represents a sample with a small initial volume fraction. This tie line connects the initial volume fraction $\phi_2 = 0.045$, with the maximum volume fraction $\phi_1 = \phi_{\max} = 0.74$ in the dense sediment. Since it is tangent to the flux curve at $\phi = 0.615$, this is the limiting tie line (largest ϕ_2) for $\phi_1 = \phi_{\max} = 0.74$. There is another shock in the sample from zero volume fraction (the clear supernatant) to $\phi_2 = 0.045$, the initial volume fraction. Since the dense sediment is constrained from moving by the cell bottom, the flux at maximum volume fraction is set equal to zero, $\phi_{\max} K(\phi_{\max}) = 0$. Thus the sample has two shocks separating three regions of different but uniform volume fraction.

These two shocks determine the lines shown in Fig. 1. The slope of the lines depends, of course, on the values of

the volume fractions on either side of the shock. For example,

$$U_{\text{sediment}} = \frac{\phi K(\phi)}{\phi_{\text{max}} - \phi} \quad (9)$$

gives the dense sediment growth velocity, where there is zero flux at the maximum volume fraction and the fluid volume fraction above the dense sediment is ϕ . Within the Kynch theory approximation, we identify the growth of the dense sediment with the crystal growth velocity $U_{\text{sediment}} = U_c$. This dimensionless crystal growth velocity is compared to data in Fig. 9. The velocity of the crystal growth increases with increasing initial volume fraction. Here the crystal grows as fast as material can be supplied. The dashed line is the velocity predicted if $\phi_{\text{max}}=0.65$ and the solid line if $\phi_{\text{max}}=0.74$. The lower dense sediment volume fraction dashed curve fits the data by Davis and Russel [9] better than the larger volume fraction solid line. Our data fit the larger volume fraction curve better, though the error is large. This comparison is another method to estimate the volume fraction of the dense sediment.

To represent physically allowed states, the tie lines in Fig. 13 must remain below the flux curve. Thus tie lines directly from the initial volume fraction to the maximum packing may be made provided the initial volume fraction is less than $\phi=0.07$, if $\phi_{\text{max}}=0.65$, and decreasing to 0.045 if $\phi_{\text{max}}=0.74$ for a flux curve determined solely by Eq. (3). For initial volume fractions greater than ~ 0.07 , the tie line to ϕ_{max} intersects the flux curve and represents an unstable condition. The tie line now must extend from the initial volume fraction to a volume fraction where it is tangent to the flux curve (line A in Fig. 13). Thus, solving

$$\frac{d[\phi_1 K(\phi_1)]}{d\phi_1} = \frac{[\phi_1 K(\phi_1) - \phi_2 K(\phi_2)]}{[\phi_1 - \phi_2]} \quad (10)$$

for ϕ_1 gives the volume fraction where the tie line is tangent to the flux curve. The other volume fraction (ϕ_2) is the initial volume fraction. There is a second tie line that is also tangent to the flux curve and extends to ϕ_{max} at zero flux. This tie line represents a shock between the dense sediment (at $\phi_{\text{max}}=\phi_2=0.65$, for example) and the less dense colloidal fluid ($\phi_1=0.51$, in this case). The predicted value of the fluid volume fraction ϕ_1 in contact with the dense sediment is highly dependent on the functional form of $K(\phi)$ and on the value of ϕ_{max} . If the form of the reduced sedimentation velocity that fits the smaller particle data better, $K(\phi) = \exp[-\phi(5.5+4.0\phi)]$, is used with the same $\phi_{\text{max}}=0.65$, then $\phi_1=0.52$. If ϕ_{max} is increased to 0.66, there is a further increase in the colloidal fluid value to $\phi_1=0.53$. However, given a unique form for the flux curve and a single ϕ_{max} Kynch theory predicts that the same volume fraction of colloidal fluid is in contact with the growing dense sediment, independent of the initial volume fraction, provided this volume fraction is greater than ~ 0.07 . Since the colloidal crystal grows in response to the fluid concentration adjacent to it, the crystal growth rate saturates and becomes constant for volume fractions greater than ~ 0.07 , as seen in Fig. 9.

Between the two (tie line) tangent points on the flux curve, there is a fan region, where the volume fraction in-

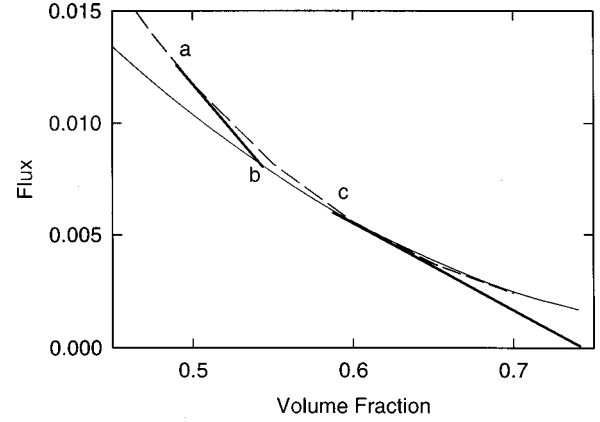


FIG. 14. Kynch theory construction including a compressible settling crystal phase. The dashed line is the metastable fluid flux curve, while the light solid line is the flux curve from the Zick-Homsey calculation. The dark solid line between *a* and *b* is the fluid to crystal shock boundary, while the dark solid line between *c* and zero flux is the shock boundary from the crystal fan to the dense crystal sediment.

creases continuously with decreasing height. In the sample each of these volume fractions ϕ moves upward in time with a velocity equal to the slope of the flux curve at that volume fraction

$$V_{\text{fan}}(\phi) = - \frac{d[\phi K(\phi)]}{d\phi}, \quad (11)$$

The predictions of Kynch theory are shown in several figures above. In Figs. 1–3 the boundary between the clear supernatant and the uniform suspension with the initial volume fraction is a line having slope $K(\phi)$ determined using Eq. (3). Equation (9) with $K(\phi)$ and $\phi_{\text{max}}=0.65$ predicts the dense sediment (crystal) boundary represented by a dash-dotted line. The crystal growth velocity depends on the initial sample volume fraction for $\phi < 0.070$. For $\phi > 0.070$, a fan is present and the fluid volume fraction in contact with the crystal is independent of the initial volume fraction. It is predicted by equating Eqs. (9) and (11) with the fan velocity set equal to the sediment velocity. The reduced crystal growth velocity is constant in this region and determined from either Eq. (9) and (11) once the fluid volume fraction is known. Thus Kynch theory rationalizes the observed crystal growth behavior displayed in Fig. 9. When there is an internal fluid/fluid shock from the initial volume fraction to denser fluid volume fraction, the shock boundary (as observed in Figs. 2 and 3) is determined by Eq. (8) using appropriate volume fraction values on either side of the shock. These internal fluid/fluid shock speeds predicted for initial volume fractions $\phi=0.0124$ and 0.22 are 0.13 and 0.17, respectively. Fitting the shock boundaries (squares) to a straight lines give experimental shock speeds 0.130 ± 0.004 and 0.18 ± 0.03 , respectively. This simple Kynch theory gives a good fit to the data.

There are problems with the previous application of Kynch theory to interpretation of the data. First, the volume fraction of the dense sediment that gives a good fit to the crystal growth velocities is $\phi_{\text{max}}=0.65$, a smaller value than the theoretical crystalline dense packing of hard spheres

(0.74) and less than all experimental estimates of the dense (crystal) sediment described earlier. Second, there is no explicit treatment of a phase transition between liquid and crystalline phases. Third, the dense sediment is assumed uniform in volume fraction, contrary to the Bragg scattering volume fraction estimates given in Figs. 11 and 12. We address these concerns in the following construction for the fluid-crystal phase transition region.

Figure 14 shows the experimentally determined flux curve for the colloidal liquid state (dashed line) extended into the metastable fluid region. Also shown is the theoretical result of Zick and Homsey [17] for a rigid face-centered-cubic lattice (solid line) that describes well the measured fluxes for settling of a polycrystalline hard-sphere solid. If we require the osmotic pressures to balance on either side of a slowly moving fluid-crystal interface (mechanical equilibrium), the crystal volume fraction may be determined in terms of the metastable fluid volume fraction by using the hard-sphere equations of state. In this way tie lines from the fluid flux curve to the crystal flux curve may be constructed as shown by the line segment *AB* in Fig. 14. The tie line represents a shock whose speed is given by Eq. (8), where ϕ_1 is the fluid volume fraction and ϕ_2 is the crystal volume fraction in the immediate vicinity of the fluid-crystal interface. The fluid volume fraction is fixed theoretically by requiring the shock speed to match the crystal growth velocity. Later we describe this matching procedure using the Williams-Frenkel growth law, which gives the crystal velocity in terms of the metastable fluid volume fraction at the fluid-crystal interface. This solves the Kynch level problem, provided a solution exists and that the solution is stable. It should be noted that Davis and Russel solve this problem in a different way [9]. They require the osmotic pressure to balance across the fluid-crystal interface, as do we. However, they require the tie line to be tangent to the fluid flux curve at ϕ_1 . Thus the fluid-crystal interface grows parallel to one of the lines of constant volume fraction in the metastable fluid fan region. The details of matching the crystal end of the tie line with the crystal flux curve are not considered. Such additional constraints would overdetermine the problem giving no solution in general.

For the moment we assume that our Kynch solution exists and concentrate on the stability of this solution. Note that for the tie line drawn in Fig. 14 the slope of the line is less than the slope of the fluid flux curve on the fluid side at ϕ_1 but more than the slope of the crystal flux curve on the crystal side at ϕ_2 . In this way the fluid, fluid-crystal, and crystal regions stay in the same order as the interface moves. The crystal region does not overtake the fluid-crystal interface, for example. This is required for stability of the construction. Furthermore, the fluid-crystal interface is asymptotically stable in the following sense. If the interface is displaced a small amount, there are no forces to return it to the original position nor to move it further away. However, as the growth continues and the fans and connecting regions expand, the relative position of the interface approaches the original position asymptotically. Corrections to the Kynch theory, with an increasing volume fraction as the interface is approached on the fluid side, will be absolutely stable for volume fractions between freezing and melting as discussed by Davis and Russel [9].

Figures 5–7 show the measured particle volume fraction as a function of height for the smaller particle samples with initial volume fractions 0.124, 0.22, and 0.44 at times 680, 760, and 760 ks after mixing, respectively. The solid lines represent the predictions for volume fraction from the Kynch theory taking crystallization into account. Of course, we expect no fit in the crystal region ($\phi > 0.5$) because no DLS correlation function measurements were made in uniform crystals as a function of volume fraction. In the upper region of the suspensions, the volume fraction is uniform and equal to the initial volume fraction. Presumably, the failure of the $\phi = 0.124$ sample to produce this volume fraction in the upper regions is due to representing the data in Fig. 4 by the best-fit straight line as shown. The sample volume fraction remains uniform down to the fluid-fluid shock region in samples with initial volume fractions 0.124 and 0.22. Then there is a sharp increase in volume fraction with height in the shock followed by a slower increase in volume fraction in the fan region, as the height in the sample decreases. No sharp increase in volume fraction, or fluid-fluid shock, is predicted or observed for the most concentrated sample with initial volume fraction 0.44. The qualitative agreement between theory and experiment is good given the limited resolution of the experimental method and the neglect of diffusion in the theory, which both contribute to a smoothing of any volume fraction discontinuities. The volume fraction variation in the fan is well represented. To plot Kynch theory for the phase transition region, we assume a reduced crystal-fluid velocity of 0.0735 to agree with the average “constant” velocity at large volume fractions (0.076 ± 0.003). Further, for purposes of illustration, we assume the theoretical maximum packing (0.74) for the crystal in the dense sediment. Under these assumptions, both the metastable fluid and the crystal volume fractions are within fan regions of their respective flux curves. Using the hard-sphere equations of state and Eq. (8) for the crystal growth velocity gives 0.500 and 0.553, respectively, for the fluid and crystal volume fractions at the phase boundary. These volume fractions extend uniformly away from the interface until intersecting the liquid or crystal fans as shown in Figs. 4–6. The velocity of the fluid fan intersection point is 0.0823, while the crystal fan intersection point velocity is 0.064. The uniform volume fraction regions on either side of the phase boundary expand in time just like the fan regions. The shock boundary from the crystal to the dense crystal sediment connects volume fraction 0.612 with 0.74 and propagates with velocity 0.039.

Decreasing the maximum volume fraction of the sediment reduces the volume fraction in the crystal fan where the shock occurs. Figure 12 shows this effect explicitly. The thick solid curve shows the Kynch theory just described and applied to the volume fraction estimates from Bragg scattering for the larger particle samples. The thin line gives Kynch theory for a maximum volume fraction 0.685, which is closer to our estimates given earlier and that value where the crystal fan is completely eliminated. For this maximum volume fraction value, there is no crystal fan predicted, only a jump from the volume fraction value at coexistence to the dense sediment value. The Kynch theory cannot describe the observed volume fraction anisotropy.

Also shown in Fig. 12 (squares) are data for an initial volume fraction below the freezing value. These crystals

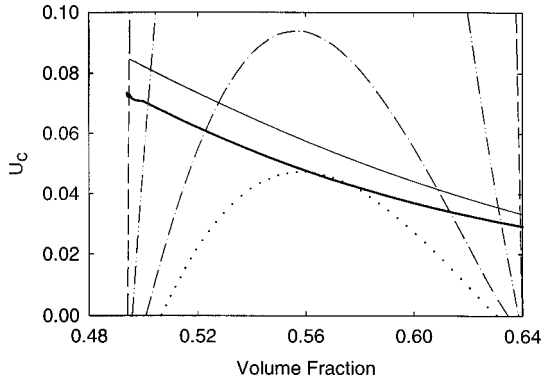


FIG. 15. Reduced crystal growth velocity [$U_c = U_g - K(\phi)$] at $Pe_p/f_0 = 0.85$ (short-dotted line), 0.49 (dash-dotted line), 0.14 (dash-double-dotted line), 0.014 (long-dashed line) as a function of metastable fluid volume fraction. The reduced liquid fan velocity is shown as a light solid line and the crystal velocity from Eq. (8) as a dark solid line. Acceptable solutions for our samples occur at $\phi = 0.523$ and $U_c = 0.61$ for the 500-nm particles at 1g and $\phi = 0.502$ and $U_c = 0.70$ for the 380-nm particles at 1g.

grow as long columns. They exhibit the same density profile as samples with initial volume fraction within coexistence region values (triangles) that produce a polycrystalline sediment. Above the dense sediment the polycrystalline solid has uniform density. The Kynch theory with a maximum packing fraction 0.74 does not produce a satisfactory volume fraction profile for either starting volume fraction. For a maximum packing fraction equal to 0.685, the theoretical profile is more representative. However, the data are much smoother than the theory. Finally, we note that the measured volume fractions appear systematically high, given the expected crystal volume fraction in the coexistence region. This value (0.545) should obtain at large times in the upper portion of the crystal before compression occurs in the fan and dense sediment, but measurements indicate a value $\sim 4\%$ larger. Alternatively, crystals homogeneously nucleated in metastable fluids are compressed by larger than equilibrium osmotic pressures. Crystals so formed may not have yet relaxed to the equilibrium volume fraction.

B. Wilson-Frenkel growth law

The Wilson-Frenkel growth law predicts crystal growth velocities that depend on the metastable fluid volume fraction ϕ in contact with the crystal interface. The growth velocity is given by

$$U_g = \frac{f_0 D_s}{R U_0} [1 - \exp(\delta\mu/k_B T)] = \frac{f_0 D_s}{Pe_p D_0} [1 - \exp(\delta\mu/k_B T)], \quad (12)$$

where $\delta\mu$ is the difference in chemical potential between the crystal and metastable liquid at the interface. We calculate this chemical potential difference, assuming osmotic equilibrium between the liquid and crystal phases, using equations of state determined from computer simulations [8,9]. The kinetic coefficient combines a particle self-diffusion constant divided by a particle radius D_s/R to estimate particle “velocities,” with a particle sticking coefficient given by f_0 [9]. Division by the dilute solution sedimentation velocity U_0

scales this velocity the same as other velocities discussed and renders it dimensionless. The observed crystal growth velocity $U_c = U_g - K_c(\phi)$ is less than the Wilson-Frenkel estimate because the crystal settles in the gravitational field.

Figure 15 presents the measured crystal growth velocity U_c , where we assume a “short-time” self-diffusion constant having the form [22] $D_s = D_0(1 - \phi/0.64)^{-1.17}$. As ϕ (the metastable fluid volume fraction in contact with the growing crystal) tends to the freezing value, the chemical potential difference and growth velocity U_g tend to zero. The growth velocity is thermodynamically limited. As the volume fraction increases above the melting value, the growth velocity decreases due to hydrodynamic drag effects. This dimensionless form of the growth velocity depends only on ϕ and Pe_p/f_0 . The growth velocity U_c is shown for several different values of Pe_p/f_0 .

When the fan curve [given by Eq. (11)] intersects the Wilson-Frenkel curve, both represent the same reduced velocity. Russel and Davis [9] argue that only the lower volume fraction of two possible intersection values is stable. Further, they argue that the lower volume fraction intersection point determines the observed crystal growth velocity. A given fan volume fraction is in contact with the crystal. The crystal grows in response to this volume fraction according to the Wilson-Frenkel law and both move together with the same velocity in a stable fashion. If the Pe_p value is increased by increasing particle size or by centrifugation, then the intersection point of interest moves to larger volume fraction until the fan curve fails to intersect the Wilson-Frenkel curve. For sufficiently large Pe_p , no crystal can grow and a glassy sediment results.

The Davis-Russel model assumes a crystal formed at the maximum dense sediment volume fraction, so they may neglect any sedimentation of the crystal in comparing theory with experiment. Furthermore, we have argued that within the Kynch theory including a liquid to crystal phase transition, there is an expanding region of uniform crystal and metastable liquid on either side of the phase boundary. The interface is not in direct contact with the fan and therefore is not constrained to match the fan velocity. However, particle number must be conserved such that the interface velocity is given by Eq. (8) using the liquid and crystal volume fractions immediately on either side of the interface. The prediction for this velocity, assuming an osmotic pressure balance across the interface, is shown in Fig. 15 as a dark solid line.

To determine f_0 within this model we centrifuged a smaller particle sample at various g values. We were careful to allow some crystal to form in the bottom under 1g before centrifugation. It is possible that nucleation of columnar crystals can be suppressed before crystal growth is suppressed. Thus pre-existing crystals eliminate nucleation constraints. The sample failed to crystallize when the centrifugation was greater than $\sim 6g$. The dotted curve in Fig. 15 corresponds to this 6g limiting value, where $Pe_p/f_0 (=0.85)$ marks the boundary between crystallization and glass formation. The corresponding f_0 value is 0.34, which agrees reasonably well with 0.27, a value determined by molecular-dynamic simulations of a Lennard-Jones fluid [23]. Using this value for f_0 determines the dash-dotted curve for the larger particle samples at 1g and the dash-double-dotted curve for the smaller particle samples at 1g.

The corresponding predicted crystal growth velocities are 0.61 and 0.70, respectively. This is somewhat lower than the observed values that lie between 0.70 and 0.80, but the narrow range of observed velocities is predicted. For Pe_p/f_0 values tending to zero, the velocity reaches a maximum value 0.735. Thus the theory has the same span in predicted velocities as seen in experiment, though smaller in absolute magnitude, for the same range in Pe_p . Using a long-time self-diffusion approximation in Eq. (12) will move the maximum velocity to smaller ϕ values and, consequently, larger velocities in Fig. 15. However, this requires unacceptably larger (by an order of magnitude) values for f_0 .

C. Beyond Kynch theory

The Kynch theory for the growth of columnar crystals with an initial volume fraction less than ~ 0.07 posits a jump from the initial volume fraction to the maximum packing fraction possible. These volume fractions lie outside the range of allowable values ($0.494 < \phi < 0.638$) used in the Wilson-Frenkel theory. As shown in Fig. 9, the velocity of the crystal phase boundary goes to zero as the initial volume fraction tends to zero. This is quite different from predictions of the Kynch theory solution in the fan region for initial volume fractions greater than 0.07. Here the Wilson-Frenkel growth law is consistent with a very narrow range of reduced crystal growth velocities, also observed experimentally as shown in Fig. 9. We wish to understand how Wilson-Frenkel theory applies to the low initial volume fraction ($\phi < 0.07$) suspensions.

Experimentally one observes a more dense colloidal fluid in contact with the growing crystal compared to the uniform colloidal fluid above. This more dense region moves up with the crystal without expanding into a fan. It is the result of diffusive broadening. Since the fluid and crystal sedimentation rates are measured and the equations of state known for hard spheres, the relative magnitude of the convective and diffusive terms may be calculated. From these calculations we expect the Kynch theory to be marginal for our samples in the crystalline phase. This explains some of the failure of Kynch theory to fit crystalline data.

The Kynch theory results from the zeroth-order equation in a large Pe perturbation expansion of the ‘‘outer solution’’ of Eq. (7) [10]. In this expansion, convection is dominant. ‘‘Resolution of the continuous variation of ϕ within the sediment boundary layer’’ requires an ‘‘inner’’ expansion [10], which scales lengths on Pe^{-1} . The zeroth-order solutions have volume fraction profiles that translate uniformly in time. Thus we assume a solution of the form $\phi(Y) = \phi(Pe[x - Lt])$ for Eq. (7) in the boundary layer regions. In this way the time derivative is replaced by a spatial derivative times $-L$. The whole equation is integrated with respect to Y to find

$$D(\phi) \frac{d\phi}{dY} = L(\phi_0 - \phi) + \phi_0 K(\phi_0) - \phi K(\phi), \quad (13)$$

where $D(\phi) = K(\phi) \{d[\phi Z(\phi)]/d\phi\}$. For the colloidal fluid region above the crystal phase boundary at low initial volume fractions or for the fluid shock region at larger initial volume fractions, ϕ_0 is the initial volume fraction and

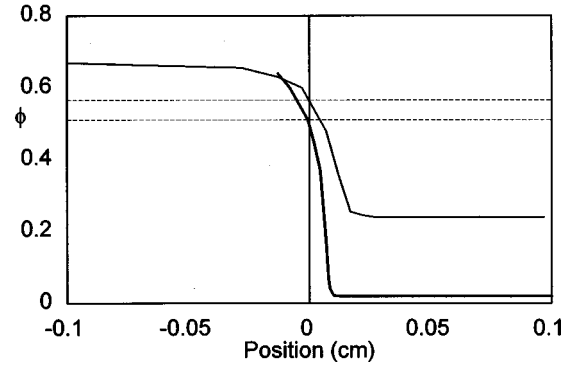


FIG. 16. Volume fraction versus sample height profile generated from Eq. (13) for the larger particle samples. The volume fractions indicated by the dashed lines correspond to crystal and fluid values that have the same theoretical osmotic pressure and reduced velocity (0.03) due to crystallization as the fluid (dark line) and crystal (light line) profiles.

$f(\phi_0) = \phi_0 K(\phi_0)$ is the flux of particles at this volume fraction. When $\phi = \phi_0$, the volume fraction is constant in spatial variable Y , as indicated by a zero-value spatial derivative. Alternatively, in the crystal phase at the sample bottom, there is a different boundary condition. The volume fraction reaches its maximum value $\phi_0 = \phi_{\max}$ and $f(\phi_0) = \phi_0 K(\phi_0) = \phi_{\max} K(\phi_{\max}) = 0$. Thus two equations, one for the fluid phase and one for the crystal phase, may be derived using appropriate boundary conditions for each phase. Similar considerations lead to an appropriate equation for the clear supernatant-uniform initial volume fraction shock profile [10]. Each of the resulting equations is integrated with respect to Y to determine (moving) spatial volume fraction profiles.

Figure 16 shows volume fraction profiles for the liquid phase (dark line) with initial volume fraction 0.0225 and the solid phase (light line) with maximum volume fraction 0.68 with $Pe = 6600$. Each solution profile represents a constant particle flux, but the flux for the solid and the liquid solutions differ in general. The reduced velocity of the shock given by Kynch theory [Eq. (8)] is 0.03 for these boundary conditions. This is also the translational velocity of both the liquid and crystal profiles if they are to move together. The motion of the shock profile represented by the phase transition must also have the same reduced velocity but given by the Wilson-Frenkel law (see Fig. 15). This latter constraint fixes the liquid and crystal volume fractions at the phase boundary to be 0.5105 and 0.5660, respectively, shown as horizontal dashed lines in Fig. 16. Thus the phase boundary is at the spatial origin in this figure. The theory predicts a dense fluid region of thickness ~ 0.01 cm in contact with the crystal. The thickness does not increase in time, as a fan does, and is consistent with experimental observations. For smaller growth velocities, the liquid volume fraction in contact with the crystal must move closer to the freezing value.

Now we consider the volume fraction profile for the crystal presented in Fig. 12. The dashed curve is a solution to Eq. (13) for a maximum crystal volume fraction 0.68. The growth or translational velocity of this profile is 0.0695 and reasonably consistent with experimental observations. We have already stated that the measured volume fractions are probably systematically large. If they are scaled to slightly

smaller values then there is good agreement with the dashed line. Both samples with initial volume fractions above and below the freezing value are shown. This first-order diffusive broadening of Kynch theory represents the data well. The solution to Eq. (13) for the maximum crystal volume fraction 0.74 produces a crystal shock boundary with much slower translational velocity, similar to the translational velocity of the Kynch theory at the base of the fan. While the data indicate crystal anisotropy, which is not included in the theory, it seems clear that there is very little crystal fan region. The maximum crystal packing must be less than 0.74 and closer to 0.68.

Further approximate solutions [10] may be developed and are quite complex. It is possible that a crystal fan is present but obscured by diffusive effects represented in higher-order approximations. Without more accurate data and a theory including crystal anisotropy, we will not develop these solutions further. However, these approximate solutions are developed with respect to the underlying Kynch theory presented here.

D. Column width issues

Figure 10 shows that the measured average width of the dense sediment colloidal crystal columns increases with increasing volume fraction. Recall that the crystal growth velocity saturates for initial volume fractions greater than 0.07 because the fluid volume fraction in contact with the crystal is the same for all samples with a fluid fan. Thus the crystal column width must be determined early in the process before the fan develops. One possible explanation is that the crystals initially laid down on the bottom of the container increase in size with increasing volume fraction. This is con-

trolled by how well particles can diffuse to crystal sites before they are locked into position by the settling of particles on top of them. This is the same argument given for the creation of a glass if the acceleration of gravity is increased beyond a certain magnitude. This argument suggests that crystals form, if there is sufficient horizontal motion (diffusion) of particles relative to the vertical settling motion. Let $S = [D_s t]^{1/2}$ be the distance that a particle diffuses horizontally in a time t . The average vertical distance the particle falls in the same time is given by $A = Ut = U_0 K(\phi)t$. Let t be the time taken to fall a particle radius R . Then with self-diffusion constants [22,24] given by $D_s = D_0(1 - \phi/\phi_{\text{lim}})^\alpha$, with $\phi_{\text{lim}} = 0.58$ and $\alpha = 1.74$ (long-dashed line), 2.6 (short-dashed line) for the short-time self-diffusion estimates and $\phi_{\text{lim}} = 0.64$ and $\alpha = 1.17$ for the long-time self-diffusion coefficients, we have

$$\frac{S}{R} = \sqrt{\frac{D_0}{U_0 R}} \sqrt{\frac{\left(1 - \frac{\phi}{\phi_{\text{lim}}}\right)^\alpha}{K(\phi)}}. \quad (14)$$

When scaled as in Fig. 10, this functional form brackets the data. However, the characteristic length given by $[D_0/U_0 R]^{1/2} = 4.5$ is two orders of magnitude too small. This argument suggests that the column length scale is determined early on in the settling process, before height inhomogeneities develop.

ACKNOWLEDGMENT

This work was supported by the National Science Foundation through Grant No. DMR 9501865.

-
- [1] P. N. Pusey, in *Liquids, Freezing and the Glass Transition*, edited by D. Levesque, J. P. Hansen, and J. Zinn-Justin (Elsevier, Amsterdam, 1990).
- [2] D. J. W. Aastuen, N. A. Clark, L. K. Cotter, and B. J. Ackerson, *Phys. Rev. Lett.* **57**, 1733 (1986); **57**, 2772(E) (1986).
- [3] J. K. G. Dhont, C. Smits, and H. N. W. Lekkerkerker, *J. Colloid Interface Sci.* **152**, 386 (1992).
- [4] Th. Palberg, R. Simon, M. Wurth, and P. Leiderer, *Prog. Colloid Polym. Sci.* **96**, 62 (1994).
- [5] J. L. Harland and W. van Meegen, *Phys. Rev. E* **55**, 3054 (1997).
- [6] K. Schatzel and B. J. Ackerson, *Phys. Rev. E* **48**, 3766 (1993).
- [7] Y. He, B. J. Ackerson, S. M. Underwood, W. van Meegen, and K. Schatzel, *Phys. Rev. E* **54**, 5286 (1996).
- [8] B. J. Ackerson and K. Schatzel, *Phys. Rev. E* **52**, 6448 (1995).
- [9] K. E. Davis, W. B. Russel, and W. J. Glantschnig, *J. Chem. Soc., Faraday Trans.* **87**, 411 (1991).
- [10] K. E. Davis and W. B. Russel, *Phys. Fluids A* **1**, 82 (1989).
- [11] K. E. Davis and W. B. Russel, *Adv. Ceram.* **21**, 573 (1987).
- [12] K. E. Davis and W. B. Russel, *Ceram. Trans.* **1B**, 693 (1988).
- [13] P. N. Pusey and W. van Meegen, *Nature (London)* **320**, 340 (1986).
- [14] S. E. Paulin and B. J. Ackerson, *Phys. Rev. Lett.* **64**, 2663 (1990).
- [15] B. J. Bern and R. Pecora, *Dynamic Light Scattering* (Wiley, New York, 1976).
- [16] G. K. Batchelor, *J. Fluid Mech.* **52**, 245 (1972).
- [17] A. A. Zick and G. M. Homsey, *J. Fluid Mech.* **115**, 13 (1982).
- [18] N. F. Carnahan and K. E. Starling, *J. Chem. Phys.* **51**, 635 (1979).
- [19] K. R. Hall, *J. Chem. Phys.* **57**, 2252 (1972).
- [20] P. N. Pusey *et al.*, *Phys. Rev. Lett.* **63**, 2753 (1989).
- [21] P. G. Bolhuis and D. S. Kofke, *Phys. Rev. E* **54**, 634 (1996).
- [22] J. S. van Duijneveldt and H. N. W. Lekkerkerker, in *Science and Technology of Crystal Growth*, edited by J. P. van Eerden and O. S. L. Bruinsma (Kluwer, Dordrecht, 1995).
- [23] J. Q. Broughton, G. H. Gilmer, and K. A. Jackson, *Phys. Rev. Lett.* **49**, 1496 (1982).
- [24] W. van Meegen and S. M. Underwood, *Phys. Rev. E* **49**, 4206 (1994).
- [25] P. N. Pusey, W. van Meegen, P. Bartlett, B. J. Ackerson, J. G. Rarity, and S. M. Underwood, *Phys. Rev. Lett.* **63**, 2753 (1989).